DGfK

Check for updates

Digitisation and Georeferencing of an Oversized Historical Map of the Bailiwick of Neuland (Winsen/Luhe) using Structure-from-Motion (SFM) Photogrammetry

Thomas Kersten[1] [ORCID] **· Leon Stößel[1] · Maren Lindstaedt[2]**

Abstract

The study of historical maps has gained significant importance in recent years due to their ability to shed light on past geographical and topographic landscapes since they serve as crucial sources for understanding past conditions. They not only provide insights into the geography and topography during the time they were created but also allow for studying long-term changes over time. In this study, an oversized historical map of the Bailiwick of Neuland from the years 1780 to 1790 was discovered in the archives of the municipal building office in Winsen an der Luhe, Germany. The map, measuring approximately 5 m × 2 m, was digitised by photogrammetric methods and subsequently georeferenced. The process involved photographing the map with two different cameras and two UAV systems at the Geodetic Laboratory of HafenCity University Hamburg. This allowed to generate a high-resolution orthophoto from each data set. The resulting orthophoto achieved a pixel size of 0.2 mm, ensuring a detailed representation of the map. To ensure accuracy, the best photo block was scaled in a bundle block adjustment using ground control points with an accuracy of 1 mm and scale bars with an accuracy of 0.1 mm. Georeferencing of the historical map was conducted using current digital orthophotos of Lower Saxony with a resolution of 20 cm. A third-degree polynomial transformation was applied during georeferencing, resulting in mean residuals of 2.5 m at the ground control points. This process ensured that the historical map was accurately aligned with the current digital orthophotos, allowing for precise spatial referencing.

Keywords Cultural heritage · Georeferencing · Map scale · Orthophoto · Structure-from-motion · Transformation

Digitalisierung und Georeferenzierung einer überdimensionalen historischen Karte der Landvogtei Neuland (Winsen/Luhe) mittels Structure-from-Motion (SfM) Photogrammetrie

Zusammenfassung

Historische Karten sind eine wichtige Quelle für Informationen über die geografische und topografische Situation zum entsprechenden Zeitpunkt in der Vergangenheit. Mit Hilfe dieses Wissens lässt sich nicht nur erforschen, wie die Geografie

✉ Thomas Kersten
thomas.kersten@hcu-hamburg.de

Leon Stößel
leon.stoessel@hcu-hamburg.de

Maren Lindstaedt
maren.lindstaedt@gv.hamburg.de

[1] HafenCity Universität Hamburg, Labor für Photogrammetrie & Laserscanning, Henning-Voscherau-Platz 1, 20457 Hamburg, Germany

[2] Landesbetrieb Geoinformation und Vermessung, Neuenfelder Straße 19, 21109 Hamburg, Germany

und Topografie zur Zeit der Karte aussahen, sondern auch, wie sich die Situation über lange Zeiträume hinweg verändert hat. Eine überdimensionale historische Karte der Vogtei Neuland aus den Jahren 1780 bis 1790 wurde in einem Spezialmagazin des städtischen Bauamtes in Winsen an der Luhe, Deutschland, gefunden. Sie misst etwa 5 m × 2 m und wurde mit photogrammetrischen Methoden digitalisiert und anschließend georeferenziert. Die Karte wurde im Geodätischen Labor der HafenCity Universität Hamburg mit zwei verschiedenen Kameras und zwei UAV-Systemen erfasst, um aus den verschiedenen Datensätzen jeweils ein hochauflösendes Orthophoto zu erzeugen. Als höchste Auflösung wurde für das Orthophoto eine Pixelgröße von 0,2 mm erreicht, und der beste Bildverband wurde mit einer Genauigkeit von 1 mm anhand von

Passpunkten und 0,1 mm anhand von Maßstäben in einer Bündelblockausgleichung skaliert. Die Georeferenzierung der historischen Karte erfolgte anhand von digitalisierten natürlichen Passpunkten in aktuellen digitalen Orthophotos mit einer Auflösung von 20 cm. Als Ergebnis für die Georeferenzierung mit einer Polynomtransformation 3. Grades wurden durchschnittliche Residuen von 2.5 m an den Passpunkten erreicht.

1 Introduction

Historical maps offer unique insights into past geographical and topographical conditions, making them invaluable sources for researchers. They provide insights into how the geography and topography appeared during specific time periods and allow for the examination of long-term changes over time. Historical maps are thus a valuable asset in various fields, including history, geosciences, social sciences, architecture, urban planning, and many others (Chen 2023). The recent discovery of an oversized historical map depicting the Bailiwick of Neuland from 1780 to 1790 in Winsen an der Luhe, Germany presents an exciting opportunity to delve into the geographical and topographical landscape of that era. With its impressive size of 5 m × 2 m and excellent state of preservation, this map not only serves as a historical cartographic document but also stands as a remarkable testimony to the past. Due to the map's enormous size and age, it is virtually impossible to display it in the museum or use it for scientific purposes. To facilitate research and ensure its long-term preservation, this map is undergoing digitization and restoration making it more readily accessible without causing any damage. The digitization process involves capturing high-resolution digital images of the historical map. Restoration efforts are also being undertaken to preserve its physical condition. These measures aim to create a digital copy that will be accessible for research purposes.

Thus, historical maps are an important source for the geographical and topographical situation at the corresponding time in the past. With the help of this knowledge, it is possible not only to research how the geography and topography looked at the time of the map but also how the situation has changed over long periods of time. Historical maps are thus a valuable asset for history, geosciences, social sciences, architecture, and urban planning (Chen 2023). In order to

facilitate research and preserve the historical map in the long term, it is useful to create a digital copy of the map. In order to preserve this cultural asset for future generations, the map is to be restored and digitally documented. This also facilitates access to the map for the public, if for example, the map is available for download at the museum's website.

For the digitisation of historical maps can be achieved through two main methods (Daniil et al. 2003): the traditional, direct method using a high-resolution scanner or the indirect method using photogrammetric techniques. The choice of method depends on factors such as map size, condition, and material sensitivity. While the scanning method using desktop publishing scanner and drum scanner is particularly suitable for maps up to DIN A0 in good condition and less sensitive, they may require calibration procedures to improve geometric quality (Baltsavias & Patias 1995; Baltsavias & Waegli 1996). On the other hand, photogrammetric scanners provide high geometric quality in the range of 1–2 micron (Baltsavias et al.1998), but may have lower radiometric quality. Photogrammetry is particularly useful for large maps or those with sensitive materials, as it allows for non-invasive digitisation and orthorectification to remove distortions. The size of the map plays a minor role for photogrammetric techniques since the process of orthorectification as a final product is the mosaicking of many individual images. In addition, orthorectification is an essential step in this process, where geometric distortions present on the map are corrected to ensure accurate representation (Daniil et al. 2003).

Structure-from-Motion (SfM) photogrammetry has emerged as a useful method for digitising historical maps due to its flexibility, cost-effectiveness, and ability to capture rich spatial information. For these reasons, structure-from-motion (SfM) photogrammetry was chosen as the digitisation method for this project. The workflow and algorithms of SfM photogrammetry are described in Luhmann (2018). The literature on SfM photogrammetry showcases its wide range of applications in various disciplines. Kersten and Lindstaedt (2012) compare open-source software and web services using SfM photogrammetry for automatic 3D object reconstruction from multiple images for architectural, cultural heritage, and archaeological applications, while Kingsland (2020) performs a comparative analysis of digital photogrammetry software for cultural heritage applications. Ballarin et al. (2015) developed an automatic system for

digitising historical maps using SfM photogrammetry with a robotic arm-mounted camera. Brandolini and Patrucco (2019) demonstrate the rapid, flexible, low-cost, and contactless nature of SfM photogrammetry in preserving and valorising valuable assets in cultural heritage.

The digitisation and georeferencing of historical maps, as well as the extraction of objects from these maps, are the subject of numerous ongoing research projects. Georeferencing is a crucial step in making data from historical maps usable in geographic information systems (GIS). It involves identifying points on the map image that have corresponding locations in reference geodata. Georeferencing historical documents can be achieved by identifying points that have remained unchanged over time and can be recognized in both the historical map and current cartography, orthophotos, or terrain data, which can serve as ground control points. Baiocchi et al. (2013) conducted a study using GPS measurements to assess the accuracy of different georeferencing strategies for historical maps of Rome. They found that the geometric quality of historical maps varies. Affek (2013) presents and discusses georeferencing methods of archival paper maps using GIS, enabling precise comparisons with contemporary reference layers. Podobnikar (2009) evaluated the quality of georeferenced maps using statistical and visual parameters. This enhanced process incorporates descriptive (textual) information about the mapping processes, derivative georeferenced data sets as land use analysis, and Monte Carlo simulations. This approach provides a more detailed understanding of the quality and consequently improves a georeferencing process for any historical data sets. Luft and Schiewe (2021) introduced content-based image retrieval to automatically locate and georeference map images from topographic map series. They aligned the maps by extracting a subset of their symbols and cross-referencing them with online reference data from OpenStreetMap. Using this method, they obtained 96% correct location predictions and a median georeferencing error of 101 m when working with the "Karte des Deutschen Reiches" at the scale of 1:100,000. Overall, these studies highlight various approaches to georeferencing historical maps and emphasize the importance of accuracy and quality assessment in this process.

Despite the oversized format and clearly visible damages, the map was also scanned in six individual parts using a high-performance flatbed scanner prior to this project. The subsequent task involved mosaicking the six singular scan parts into a seamless map. This allowed for a comparison of the results between the two digitization processes – SfM photogrammetry versus desktop publishing scanning.

This paper provides a summary of the digitisation and georeferencing process of an oversized historical map of the Bailiwick of Neuland near Winsen an der Luhe in Germany, using photogrammetric methods. The structure of the paper is as follows. The introduction in Sect. 1 provides an overview of the topic and includes a review of related work on digitization and georeferencing of historical maps. The historical map of the Bailiwick of Neuland is described in Sect. 2, including its size and any notable features. In Sect. 3 the photogrammetric data acquisition using different digital camera systems is presented, while the comprehensive processing steps for handling the acquired image data are summarised in Sect. 4. The subsequent georeferencing process for both the generated orthophotos and the scanned map is explained in Sect. 5, while results obtained from the georeferencing process are analysed and discussed in Sect. 6. Finally, important findings and lessons learned during the digitization and georeferencing process including an outlook on potential future work such as vectorisation of historical maps are presented in Sect. 7.

2 The Historical Map of the Bailiwick of Neuland

The hand-drawn historical map of the Bailiwick of Neuland (Fig. 1) provides a detailed representation of the topography and geographical features of the area, including the town of Winsen an der Luhe and its surroundings. The map, measuring approximately 5×2 m, offers insights into the landscape and land use at the time it was created. The map includes various topographic elements such as rivers, ditches, roads, settlements with individual buildings, land boundaries, and prominent terrain formations. It also depicts agricultural fields, which are predominantly rectangular and elongated in shape, with numbering for identification purposes. This provides information about the agricultural practices and land division in the area during that period. Additionally, four profile lines with point designations can be found on the map. These profiles extend across large areas of the depicted region, particularly close to the river Elbe. According to the map's description, the associated profiles can be found on a separate tear that has also been digitised and is available through Arcinsys Lower Saxony and Bremen—an archival information system. The scale of this sketch is 1: 1900, and it was produced in a format measuring 49×464 cm according to information from Niedersächsisches Landesarchiv (2022). Furthermore, there is a profile of a dike in the lower part of the map, accompanied by a line indicating its desired height. Given that the Bailiwick of Neuland had to address drainage issues and protect against floods from the nearby Elbe River, these profile lines and dyke profiles likely relate to these concerns (Seebach 1955).

According to the map's description, it was recorded between 1780 and 1790 by engineer Major Schneider. The map's units of measurement are based on the Calenberg region, specifically the Calenberger Morgen. The term "Morgen" refers to a historical German unit of area that

Fig. 1 The historical map of the Bailiwick of Neuland in Winsen/Luhe, Germany

varied across different regions. In the Calenberg region, one Calenberg acre is composed of 120 Calenberg square rods (von Schlieben 1857). To convert these units into meters, the following conversions can be used (Kost 1955): 1 Calenberg rod = 4.674 m, 1 Calenberg foot = 0.292 m, and 1 Calenberg inch = 2.434 m. By squaring the rods and multiplying by the factor of 120, the area of the Calenberger Morgen is approximately 2621 m^2. The map includes a total of six scales. Four scales are located near the corners of the map, representing the scale of 110 Calenberg rods to the ground plan. Additionally, there are two scales positioned to the right and left of the dike profile, indicating the scale of 55 Calenberg feet and 60 Calenberg feet for the heights of the profile. These scales provide a reference for understanding distances and measurements depicted on the map in relation to their real-world counterparts in terms of Calenberg units of measurement.

The historical map of the Bailiwick of Neuland does not provide any details or references to the map projection used. However, it was drawn around the same time as the Kurhannoversche Landesaufnahme, a land survey of the electorate of Hanover that took place between 1764 and 1786 (Kost 1955). The Bailiwick of Neuland was also completely recorded as part of this land survey. The maps produced during the Kurhannoversche Landesaufnahme did not utilize a specific map projection. Instead, they assumed a flat surface for the earth's surface, which allowed for practical accuracy in terms of distance, angle, and area (Kost 1955). It can be inferred that the cartographic methods used for the historical map of the Bailiwick of Neuland were similar to those employed during the Kurhannoversche Landesaufnahme. Given the geographical and temporal similarities between these projects, it is reasonable to assume that the historical

map of the Bailiwick of Neuland also considered a flat surface as its reference area and did not employ a specific map projection.

Another set of maps that can be compared to the historical map of the Bailiwick of Neuland is the Oldenburg Bailiwick maps, which were created between 1781 and 1799. These maps underwent investigations into their geometric accuracy by comparing six of them, at a scale of 1:3000, with the cadastral map from the state survey conducted in 1836. To carry out this comparison, a similarity transformation was employed, and the average positional error ranged from 10 to 40 m (Kost 1955). This indicates that there were some discrepancies between the Oldenburg Bailiwick maps and the later cadastral map.

As mentioned in the introduction (Sect. 1), the historical map of the Bailiwick of Neuland had already been digitised by the company Galerie Deichstraße in Hamburg, Germany, using a flatbed scanner before this project started, but it had not been georeferenced. According to the information from the company, the digitisation was carried out with a Cruse CS 220 St1100 scanner in six individual scans since the scanning area is limited to 180 cm × 120 cm. The resolution is 300 dpi, which corresponds to 0.08 mm/px. The individual scans were then digitally mosaicked to a complete image. The scanner has a suction plate so that the map is securely held flat on the flatbed table during the scanning process. The geometric accuracy of the scanned map was investigated and compared to the results of photogrammetric orthophotos.

Fig. 2 Image data acquisition with UAV system DJI Phantom 4 Pro (left) and with Nikon D7500 at the telescopic rod

3 Photogrammetric Data Acquisition

The photogrammetric image acquisition was carried out on May 24th, 2023, in the geodetic lab of the HafenCity University Hamburg (Fig. 2). The map of Bailiwick of Neuland, which was rolled up on the short side, was unrolled on the floor and laid out as flat as possible. Metal rails and levelling rod bases were placed along the edges of the map for weighting. In addition, levelling rods were placed on the long sides and on one short side of the map to be used for scaling the photogrammetric images. Therefore, the data acquisition process is divided into photogrammetric image recording and tachymetric measurements for determining ground control points (GCP) on the map and surroundings. The measurements of the GCPs were conducted immediately after the photogrammetric recording using five different camera systems (Table 1). The photographs were taken in aperture priority mode with a consistent, pre-determined aperture value. Due to the varying camera height, which was low but still inevitably different, all images were automatically focused. The lighting conditions remained similar throughout the photography process, with natural light coming through the windows and artificial light from the ceiling lighting in the lab. The number of images taken for each camera is summarised in Table 1.

The recording process began with the use of UAV systems. Initially, the DJI Mavic Air 2S was employed at a flight altitude of approximately 1 m. However, the wind generated by the rotor blades of the UAV caused slight swirling of the map both at the outer edges and in the central area. Therefore, the flight was stopped, and nadir images were then captured at three different flight heights for better camera calibration: around 1.8 m, 2.2 m, and 2.5 m. It was not possible to increase the flight altitude further due to the height of the ceiling and the undesired decrease in ground resolution. Subsequently, the DJI Phantom 4 Pro was used for another flight at a flight altitude of approximately 2.5 m. The larger size of this UAV system resulted in increased swirling of the map. Both UAV systems captured additional oblique images, which were necessary to enhance the accuracy of simultaneous camera calibration parameters. The flight configurations of these two UAV systems are depicted in Fig. 3.

Table 1 Camera systems used for photogrammetric image recording

	DSLR Nikon D7500 (with telescopic rod)	DSLR Nikon D800 (handheld)	UAV DJI Mavic Air 2S	UAV DJI Phantom 4 Pro
Sensor	CMOS	CMOS	CMOS	CMOS
Focal length [mm]	20/50	20	8,8	8.8
#Pixel	5.568×3.712	7.390×4.912	5.472×3.648	5.472×3.648
Pixel size [µm]	4.22	4,86	2.4	2.4
Sensor size [mm]	23.5×15.6	35.9×24.0	13.13×8.75	13.13×8.75
Aperture	f/7.1	f/7.1	f/2.8	f/2.8
ISO	400	400	100—110	400
#Images	62/121	71	174	81
Photo scale (average)	1:110/1: 53	1: 73	1: 284	1:259
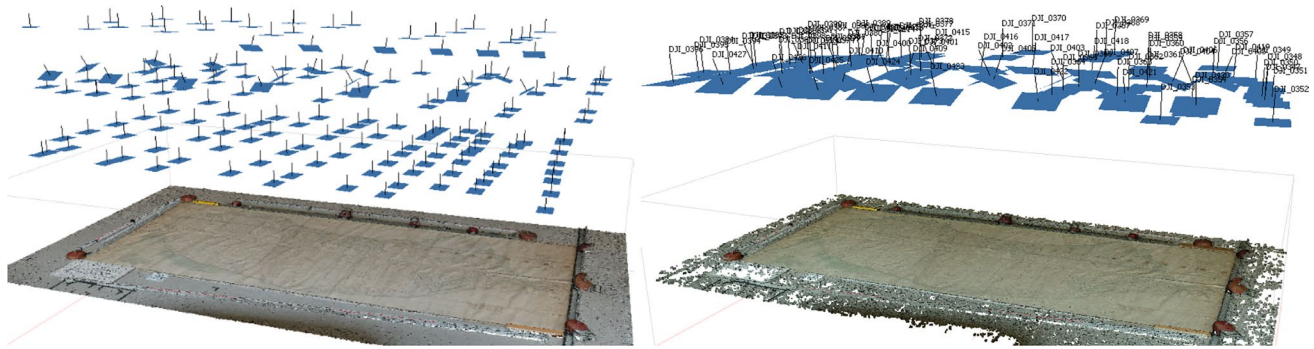
Fig. 3 Flight configurations of the two UAV systems—DJI Mavic Air 2S (left) and DJI Phantom 4 Pro (right)

Nadir and oblique images were captured using the Nikon D7500 DSLR camera mounted on a telescopic rod. The 20 mm lens was used at a height of 2.5 m, while the 50 mm lens was used at a height of 2.75 m. To remotely control the camera on the telescopic rod and adjust shooting parameters, a smartphone with the free SnapBridge app from Nikon was utilized. This app also provided a live view of the scenery on the camera display. The final set of images was taken with the Nikon D800 DSLR. However, in this case, the camera was handheld at a height of approximately 1.5 m without the use of the telescopic rod. The Nikon D800 does not have smartphone app control capability. The image block configurations for the DSLR cameras are depicted in Fig. 4. The photo scale of these five data sets varies from 1: 53 to 1: 284 (Table 1).

In the final step of the data acquisition process, 24 ground control points were measured using the Leica total station TS16, which has a technical specification that allows for a planimetric precision of approximately 2 mm. These GCPs were measured on prominent positions on the map (natural features), such as where parcel markings intersected, where lines intersected, or other precisely defined topographic features. Additionally, four GCPs were measured on the levelling rods located outside the long sides of the map. These control points served as reference points of scaling the photogrammetric images. An overview of all the measured control points can be seen in Fig. 5.

4 Photogrammetric Data Processing and Results

The five photogrammetric image data sets were processed using the software Agisoft Metashape 1.8.4. After the automatic alignment (orientation) of the images and the manual measurements of the ground control points, the bundle block adjustment was carried out to determine the precise image orientation and the camera calibration parameters using feature points (tie points) resulting in a sparse point cloud. To improve the results, gross measurement errors were eliminated using different filter in Metashape. Filtering of gross measurement errors in the sparse point clouds result in a reduction of the number of tie points by a factor between 2.3 and 3.3 (Table 2). A high reprojection error indicates problems with the localisation of point projections as well as false matches in the images. By removing points with a high reprojection error, the geometry can be improved, and thus also the orientation of the images.

The most relevant results of bundle block adjustment for all image data sets of the respective camera systems are listed in Table 3. The ground resolution (ground sampling distance GSD) is also included ranging from 0.2 and 0.7 mm, as it affects the accuracy of image orientation. The UAV systems, DJI Mavic Air 2S with 0.55 mm/px and DJI Phantom 4 Pro with 0.68 mm/px, achieved the lowest GSD due to their focal length and flight altitude. On the other hand, the Nikon D7500 dataset using the 50 mm lens obtained the highest
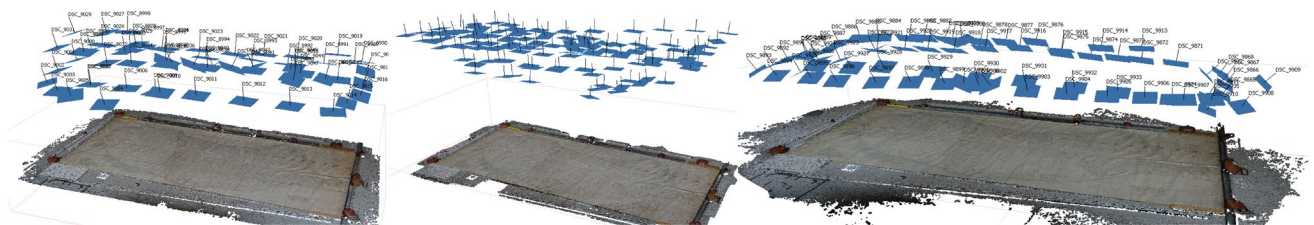
Fig. 4 Image block configurations of Nikon cameras—f.l.t.r. D7500 (20 mm), D7500 (50 mm), and D800 (20 mm)
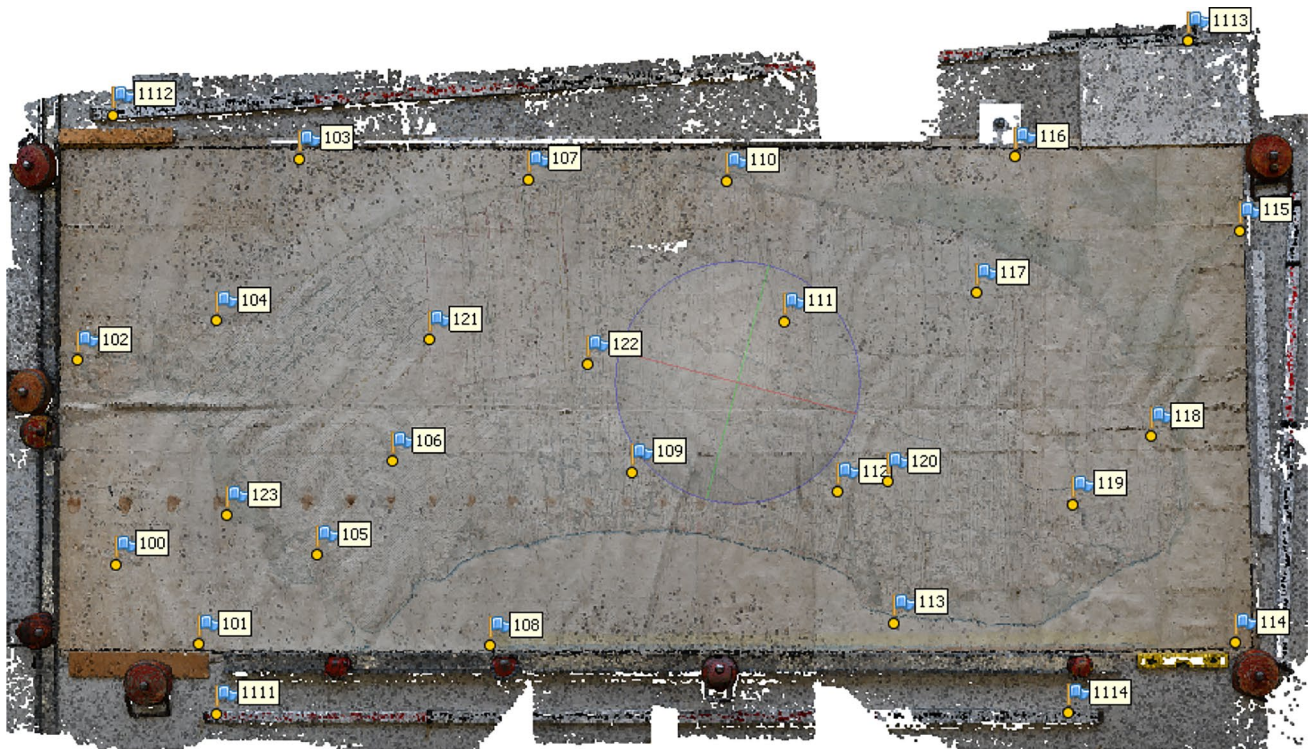
Fig. 5 Distribution of the determined ground control points (natural features) on and around the map (on the levelling rods)

Table 2 Number of tie points (sparse point cloud) before and after filtering as well as reprojection error per data set

System	# Images	# Tie points unfiltered	# Tie points filtered	Reduction factor	Max. reprojection error [px]
D7500/20 mm	62	67.756	29.845	2.3	0.20
D7500/50 mm	121	163.882	62.992	2.6	0.17
D800/20 mm	71	90.676	29.605	3.1	0.28
Mavic air 2S	174	159.597	67.369	2.4	0.68
Phantom 4 Pro	81	74.309	22.293	3.3	0.30

Table 3 Ground sampling distance (GSD) as well as residuals of the ground control points (GCPs) and scale bars (SB) per data set

System	GSD [mm/px]	Root Mean Square (RMS) GCP [mm]					RMS SB [mm]
		X	Y	Z	XY	XYZ	
D7500/20 mm	0.46	0.87	0.66	0.46	1.09	1.18	0.29
D7500/50 mm	0.21	0.81	0.65	0.74	1.05	1.28	0.12
D800/20 mm	0.37	0.93	0.81	0.76	1.24	1.45	0.40
Mavic Air 2S	0.55	1.10	0.74	0.86	1.30	1.58	0.39
Phantom 4 Pro	0.68	0.96	0.78	0.70	1.24	1.42	0.18

GSD of 0.21 mm/px. The root mean square (RMS) of the GCPs for all data sets is less than 1 mm for each coordinate, approximately 1.2 mm for XY and 1.4 mm for Z, and on average lower than the estimated a priori standard deviation of 2 mm. The accuracy achieved for the scale bars is several factors higher than the ground control point accuracy for all data sets due to the clear definition of the measured points.

The highest accuracy was achieved with the D7500 (50 mm lens) at a value of 0.12 mm. The values of the other data sets range between 0.18 mm and 0.4 mm due to the different photo scale (Table 1). However, it should be noted that different distances were measured for the scales in some cases, so the values are not directly comparable. In summary, it can be concluded that the best result was achieved with the

Fig. 6 Number of points (in million) in the generated point clouds of the respective data set

Nikon D7500 / 20 mm — 24,466
Nikon D7500 / 50 mm — 100,690
Nikon D800 / 20 mm — 38,815
DJI Air 2S — 21,246
DJI Phantom 4 Pro — 11,083
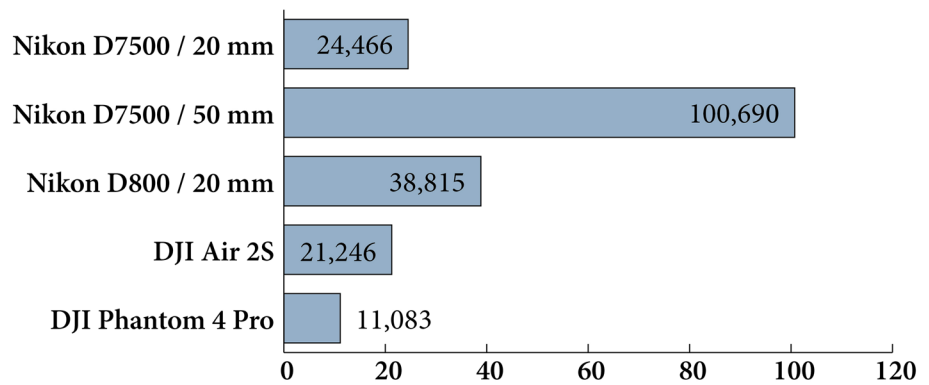
Nikon D7500 (50 mm lens) due to the camera parameters (focal length and distance to object) and the resulting GSD.

Simultaneous calibration of the interior orientation parameters for each camera through bundle block adjustment is crucial for achieving high accuracies in object space using image data. While a detailed analysis of the camera calibration results is beyond the scope of this discussion, it can be summarized that the interior orientation parameters were accurately determined for each camera. The camera calibrations also demonstrated that very low standard deviations for the focal length can be achieved for image blocks with shots at different heights above the map and with oblique shots. This in turn has an impact on the accuracy of the height coordinate and influences therefore also the accuracy of the pixel position in the orthophoto. For a comprehensive description of the camera calibration process for the five cameras used in this project, refer to Stößel (2023).

The next step involved calculating dense point clouds for each data set using the previously oriented images. Agisoft software Metashape was used to first calculate depth images through Dense Stereo Matching for overlapping image pairs. These depth images are then merged to create a combined depth image for each individual image. Based on these combined depth images, partial dense point clouds were calculated, which were subsequently merged to create a complete dense point cloud. The RGB colours of the points are sampled from the corresponding images.

In this processing step, two settings can be adjusted: the quality of the dense point cloud and the strength of the depth filtering. The quality level determines the density and accuracy of the calculated point cloud. In this case, the quality level was set to high, which reduces the resolution of the captured images by a factor of 2. This setting strikes a balance between point precision, which is sufficient for this application, and computation time. The strength of the depth filtering determines how outliers are eliminated. For this project, the depth images were calculated with the parameter set to mild, which is recommended by the software manufacturer for detailed objects. This setting helps to remove outliers while preserving detailed information in the point cloud.

The point clouds generated from the images of the different camera systems, using the same processing parameters, primarily differ in the number of points. This can be observed in Fig. 6 of the diagram. The point cloud generated from the Nikon D7500 dataset with a 50 mm lens has the highest number of points, exceeding 100 million points in total. On the other hand, the dataset from the DJI Phantom 4 Pro generated the lowest number of points, with just 11 million points. This difference can be attributed to factors such as the number of images captured and the distance to the object being surveyed.

Before calculating the digital orthophotos for each dataset, a digital surface model (DSM) of the map is required. The previously calculated dense point cloud is used as the data source for 3D triangulation to generate meshes of the DSM. The digital surface models are then calculated for each dataset with a ground resolution that is two times lower than that shown in Table 3. The ground resolutions range from 0.41 mm/px for the Nikon D7500 with a 50 mm lens to 1.37 mm/px for the DJI Phantom 4 Pro. An example of the digital surface model can be seen in Fig. 7. This particular DSM was generated from the dataset captured by the Nikon D7500 with a 20 mm lens. It clearly shows that the map was not flat but rather wavy and uneven on the ground of the lab. These digital surface models are necessary for the orthogonal rectification of the oriented images, ensuring accurate alignment with the terrain features.

The pixel size of the orthophoto suggested by Agisoft Metashape corresponds to the average ground resolution of the images. The process of orthophoto production is described in detail by Luhmann et al. (2020). In contrast to the digital surface models, the digital orthophotos were calculated using the ground resolution listed in Table 3. For each data set, an identical orthophoto section is shown in Fig. 8. At first glance, it is evident that the dataset captured by the Nikon D7500 with a 50 mm lens provides the highest ground resolution. Details such as writing or fine lines are most sharply recognizable in this orthophoto. On the other hand, this level of detail is not clearly visible in the orthophoto generated from the DJI Phantom 4 Pro

Fig. 7 Exemplary digital surface model of the map generated from the data set of the Nikon D7500 with 20 mm lens to show the unevenness of the map

-1.27 m

-1.35 m

-1.43 m

1.12 m
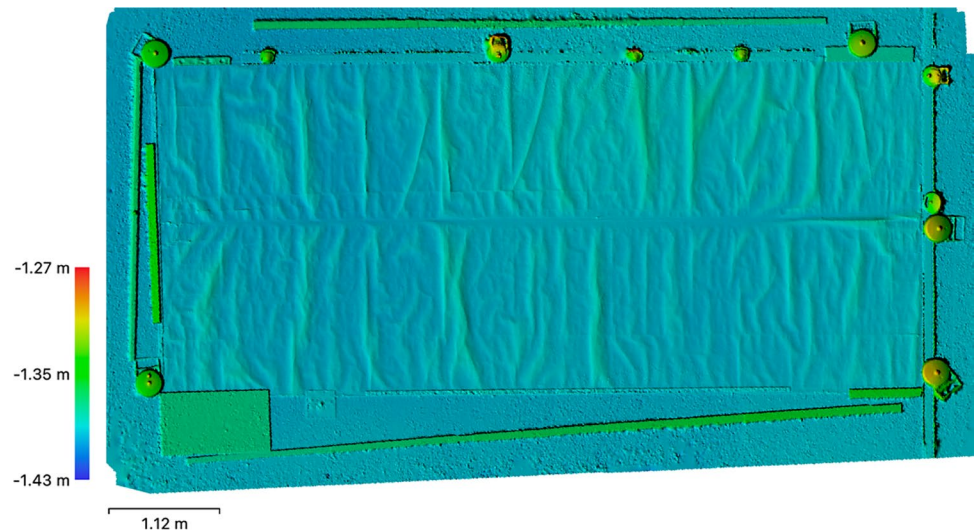
(a) Nikon D7500 (20 mm)　　(b) Nikon D7500 (50 mm)　　(c) Nikon D800 (20 mm)
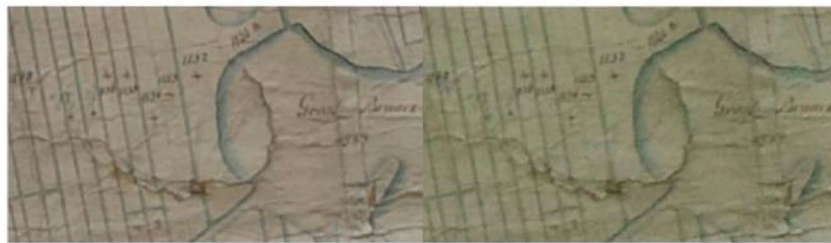
(d) DJI Air 2S　　(e) DJI Phantom 4 Pro

Fig. 8 Identical image section of the digital orthophotos of the respective camera systems (**a**–**e**)

dataset. Additionally, there are noticeable radiometric differences when comparing individual orthophotos. Furthermore, some areas appear blurred in the orthophotos of the DJI Air 2S and Nikon D800 datasets. These blurred areas may be due to factors such as motion blur during image capture or limitations in image quality.

5 Georeferencing of the Orthophotos and the Scanned Map

The georeferencing process involved using the georeferencing tool in QGIS, which is a software program formerly known as Quantum GIS (Flenniken et al. 2020). The first step was to create a new project in QGIS, specifying the coordinate system as ETRS89/UTM zone 32N (EPSG:25832). This coordinate system was defined by the Landesamt für Geoinformation und Landesvermessung Niedersachsen (2023) and is commonly used for mapping and spatial analysis in the region. Once the project was set

up with the appropriate coordinate system, the next step was to georeference the orthophotos and scanned map into the UTM coordinate system using the georeferencing tool in QGIS.

By using GCPs, which are identifiable features common to both the digital data and the real-world reference system, the georeferencing tool performs a coordinate transformation to accurately position the digital data in geographic space. In this case, GCPs were selected by comparing features in the orthophotos captured by different cameras and lenses with corresponding features in the historical map and current digital orthophotos of Lower Saxony.

After creating the new project in QGIS with the specified coordinate system, current digital orthophotos (DOP20) of Lower Saxony were added as WMS layers. These orthophotos have a ground sampling distance (GSD) of 20 cm and a positional accuracy of 0.4 m according to AdV (2020). To aid in the search for suitable GCPs, a topographic map from 1880 was also imported into the project. The georeferencing process started with the orthophoto captured by the Nikon D7500 with a 50 mm lens, which had the highest resolution among the photogrammetric orthophotos. This orthophoto was used to search for suitable GCPs in both the historical map and the current DOP20 orthophoto. Identifying appropriate GCPs proved challenging, but the corner points of Winsen Castle, which is over 700 years old, were identified as unchanged reference points. One of these corner points was measured and used as a ground control point (No. 0). Other control points were defined by corners of parcel boundaries (No. 1, 4, 6, 11, 12, 14), field boundaries, or crossing ditches (No. 2, 3, 5, 7, 8, 9, 10, 13, 15). To validate the correctness of GCPs at parcel boundaries, comparisons were made with today's land register map. Figure 9

illustrates the distribution and location of the GCPs on the map. Detailed views of all ground control points are shown in Fig. 10, both in the DOP20 section (top) and the historical map section (bottom). These visualisations provide a clear representation of the identified GCPs and their correspondence between different datasets.

It was particularly challenging to locate suitable ground control points in the upper part of the map shown in Fig. 9, as the landscape has undergone significant changes and there is little correspondence with the current situation. Nonetheless, a total of 16 identical points was identified that can serve as ground control points for georeferencing. These GCPs differ from those in Fig. 5, as these points (Fig. 9) are used for the 2D transformation between map and orthophoto, while the others (Fig. 5) are used to determine the image orientation in the bundle block adjustment. In the next step the georeferencing was calculated for each data set using both a Helmert transformation and a third-degree polynomial transformation. While the Helmert transformation (a similarity transformation) determines only two shifts, one scale and one rotation, the polynomial transformation (3rd degree with 20 parameters) allows for more complex distortions of a grid and can be used to describe non-linear deformations. According to Podobnikar (2009), polynomial transformations and spline transformations (rubbersheeting) are commonly used methods for georeferencing maps. Therefore, the results of both transformation methods can be compared and analysed as follows. In terms of the grey value interpolation method, the Nearest Neighbour variant produced significantly better visual results compared to alternatives such as linear, cubic, or cubic spline functions. As a result, Nearest Neighbour was selected for grey value interpolation. The orthophoto output raster was saved as a GeoTIFF file. The aforementioned processing steps were applied to all

Fig. 9 Overview of the distribution of all measured ground control points (note: map is oriented to the north here in contrast to Fig. 1)
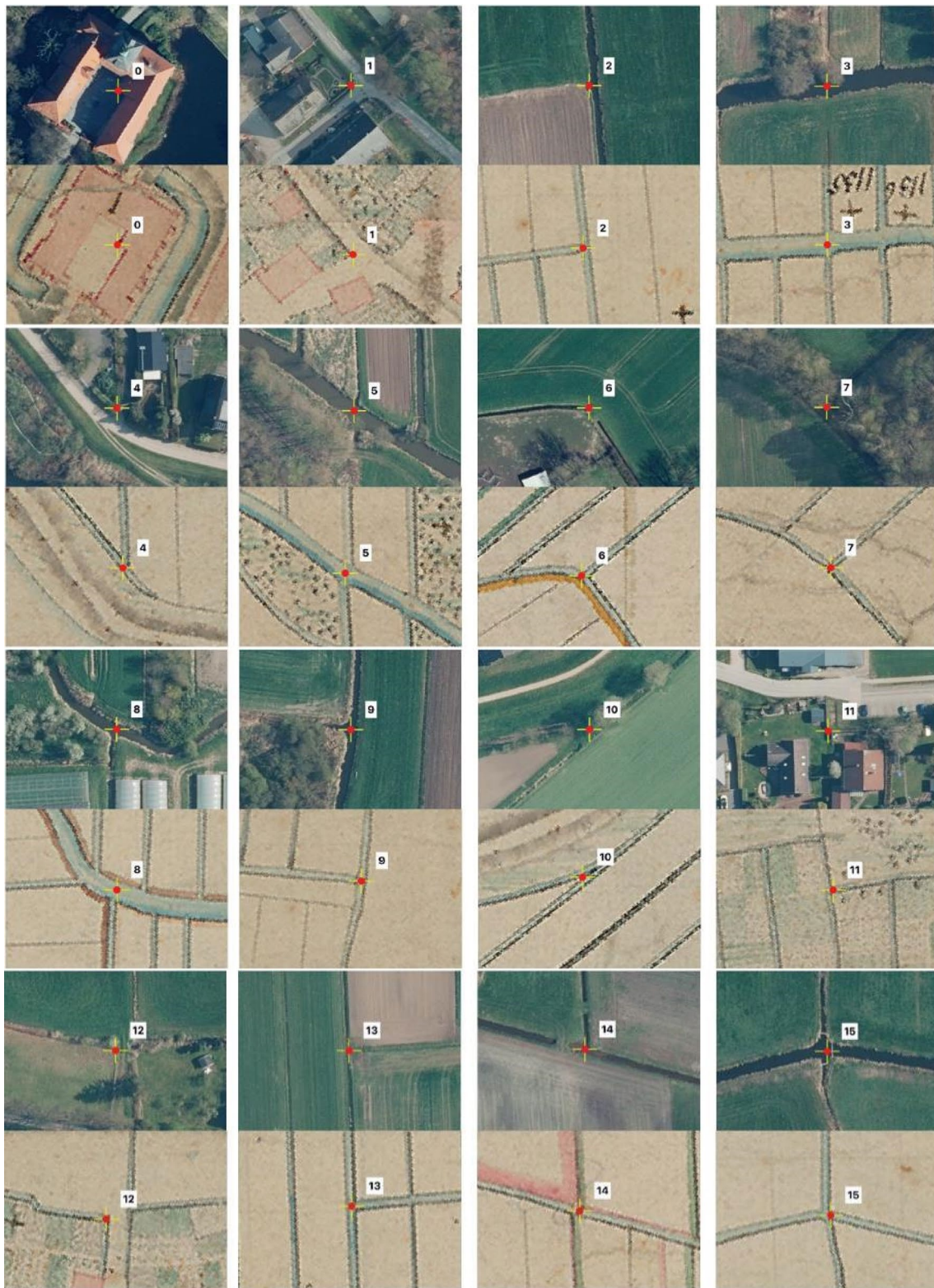
Fig. 10 Overview of all ground control points for georeferencing. On top in each case: DOP20-Sect. (2020), below in each case: historical map Sect. (1780-1790)

Table 4 Results of georeferencing using Helmert transformation (left) and polynomial transformation (right) for each data set

	Helmert transformation - Residuals of the control points [m]							Polynomial transformation - Residuals of the control points [m]					
Point no.	D7500 / 20 mm	D7500 / 50 mm	D800 / 20 mm	Mavic Air 2S	Phantom 4 Pro	Scanned map	Point no.	D7500 / 20 mm	D7500 / 50 mm	D800 / 20 mm	Mavic Air 2S	Phantom 4 Pro	Scanned map
0	13,41	13,54	13,13	13,04	13,08	178,42	0	0,65	0,66	0,63	0,43	0,53	1,47
1	4,88	4,97	4,74	5,14	3,39	29,09	1	3,81	3,87	4,04	3,40	3,95	3,32
2	3,58	3,62	3,25	2,12	3,41	35,43	2	3,70	3,90	2,95	2,91	3,39	2,89
3	2,91	2,89	2,88	2,67	2,56	37,31	3	1,24	1,29	1,15	1,37	0,93	0,59
4	9,71	9,71	10,09	10,44	9,64	67,49	4	2,42	2,55	2,42	2,24	2,22	3,35
5	13,60	13,70	14,19	13,23	15,26	44,25	5	5,93	6,15	6,02	5,67	6,28	2,52
6	2,15	2,16	2,60	3,13	2,66	24,04	6	1,74	1,71	1,53	1,17	1,50	3,82
7	7,87	7,80	7,86	8,01	9,30	46,34	7	2,67	2,88	2,79	2,77	2,66	0,94
8	7,49	7,64	7,35	7,64	7,90	42,32	8	2,38	2,37	1,74	2,45	1,99	1,42
9	4,65	4,31	5,03	5,42	4,63	22,08	9	2,49	2,61	2,06	1,73	2,26	4,04
10	2,45	2,40	2,61	3,34	1,98	42,28	10	4,75	4,81	5,05	4,27	4,97	3,78
11	7,28	6,66	7,72	7,48	6,96	43,18	11	1,42	1,35	1,37	1,47	1,27	1,46
12	4,69	5,03	4,85	4,99	5,20	46,93	12	3,12	3,30	3,13	2,87	2,87	4,46
13	4,86	5,12	4,74	4,62	5,46	19,64	13	3,07	3,05	3,06	2,79	3,52	1,66
14	2,75	2,66	2,86	2,81	2,49	66,53	14	1,54	1,54	1,54	1,66	0,81	3,14
15	1,86	1,76	1,49	2,44	1,74	19,52	15	0,38	0,57	0,81	0,88	0,45	0,79
Mean value [m]	5,88	5,87	5,96	6,03	5,98	47,80	Mean value [m]	2,58	2,66	2,52	2,38	2,48	2,48
Total error [m]	7,39	7,39	7,50	7,47	7,66	64,31	Total error [m]	4,82	4,97	4,76	4,42	4,81	4,52
GSD [m]	0,89	0,68	0,72	1,08	1,34	0,68	GSD [m]	0,88	0,68	0,71	1,07	1,32	0,67

Residuals of the ground control points per column coloured according to the size of the deviations. White is lowest deviation per column, red is highest deviation per column

orthophotos and the scanned map using the same settings. However, to facilitate data processing in QGIS, the resolutions of both the scanned map and the orthophoto taken with a Nikon D7500 camera and a 50 mm lens had to be reduced. The resolution of the scanned map was decreased from 300 to 72 dpi using Adobe Photoshop, while the ground resolution of the orthophoto was reduced from its original value of 0.21 mm/px to 0.35 mm/px in QGIS. This adjustment ensured that both datasets had approximately the same resolution.

The results of the georeferencing for each data set's individual GCPs, as well as the total error, are summarized in Table 4 for both the Helmert transformation and the polynomial transformation of the 3rd degree. To facilitate clearer comparisons and better highlight differences between the data sets, the residuals of the GCPs per data set (column) are color-coded based on the magnitude of deviations. White represents the lowest deviation per column, while red represents the highest deviation. When comparing to the Helmert transformation, it can be observed that the polynomial transformation yielded the best result for georeferencing (refer to Table 4).

The mean value of the residuals for the GCPs is 6.0 m for all orthophotos derived from photogrammetry using the Helmert transformation. However, the scanned map has a significantly higher mean value of 47.8 m. On the other hand, when using the polynomial transformation, the mean value is approximately half at around 2.5 m for all data sets (refer to Table 4). In QGIS, the total error is calculated by dividing the sum of squares of the residuals of the GCPs by the difference between the sum of ground control points and the minimum number of GCPs required for the transformation (2 for Helmert and 10 for 3rd degree polynomial). The

square root of this result is then taken. Using the Helmert transformation, the total error for each data set is worse by a factor of 1.3 compared to the mean value of the residuals. However, when using the polynomial transformation, this factor increases to 1.8. The ground sampling distance (GSD) was computed by multiplying the pixel resolution with the map scale of 1:1950 (as mentioned in Sect. 6). This results in GSDs ranging from 0.7 m to 1.3 m for both the scanned map and rectified image data.

The georeferencing of the scanned map yielded different results. When computing the Helmert transformation, the residuals of the GCPs ranged from 20 to 178 m. This indicates that the geometric inaccuracies of the scanned map could not be adequately compensated for by the Helmert transformation with four parameters. In comparison to the orthophotos generated through photogrammetry, the mean value of the residuals for the scanned map is significantly higher at 48 m. Additionally, the total error for the scanned map is 64 m. However, the polynomial transformation was able to effectively compensate for the deformations in the scanned map, achieving similar values as all orthophotos generated through photogrammetry (refer to Table 4).

6 Analysis and Discussion

To assess the precision of the photogrammetric data processing, including the bundle block adjustment with camera calibration, the mean standard deviation of the GCPs is relevant (refer to Table 3). In this case, results ranging from 1.18 mm to 1.58 mm for XY position and Z height were achieved. These values indicate a higher level of precision compared to the estimated precision of 2 mm for the GCPs

measured by tachymetry. Furthermore, the root mean square (RMS) of the scale bars is very low, ranging from 0.12 mm to 0.40 mm due to clear point definition. This represents a very good photogrammetric result in terms of accuracy. Another important aspect of assessing photogrammetric precision is the determination of interior orientation parameters through simultaneous camera calibration. According to Luhmann et al. (2020), the standard deviation for determining the focal length (c) and principal point x_0 and y_0 should be within the range of image point measurement precision, which is typically between 0.2 px and 0.5 px. For all camera systems except for the DJI Phantom 4 Pro, these values could be achieved. The DJI Phantom 4 Pro had a higher standard deviation of 1.5 px due to its weak image flight configuration. Simultaneous camera calibration in Metashape determines reliably and significantly all systematic image errors such as radial distortion, tangential distortion, affinity, and shear for all image datasets (Stößel 2023).

The orthophotos generated from photogrammetric image data were able to be georeferenced with high accuracy using both the Helmert transformation and the third-degree polynomial transformation. The differences of all photogrammetric datasets and transformation types were within a few decimetres. With the Helmert transformation, accuracies of approximately 6.0 m for the mean value of the ground control point residuals and 7.5 m for the total error were achieved. On the other hand, the 3rd degree polynomial transformation yielded lower accuracies, with a mean value of 2.5 m for the ground control point residuals and a total error of 5.0 m. When considering the accuracy of comparable maps, such as the Oldenburg Vogtei maps with an accuracy between 10 and 40 m (as mentioned in Sect. 2), these results indicate a high level of geometric accuracy for both the map itself and the georeferencing method used. However, it is worth noting that the georeferencing of the scanned map showed geometric deviations that were eight times higher than those observed for the photogrammetric orthophotos. These geometric deformations were likely caused by the mosaicking process of six individual scans into one image and by the performance limitations of the scanning system. Fortunately, these deformations could be effectively compensated for using the polynomial transformation.

When comparing the photogrammetrically recorded data and their subsequent georeferencing, it can be concluded that the georeferenced orthophoto of the dataset captured by the Nikon D7500 with a 50 mm lens is of the highest quality. This is due to the significantly higher ground resolution achieved in this dataset compared to the others. The ground resolution in this dataset is approximately 0.41 m/pixel, whereas in the other datasets it is around 0.68 m/pixel. A higher ground resolution allows for more detailed features to be clearly visible on the map. In terms of georeferencing method, the 3rd degree polynomial transformation is recommended as it yields the lowest deviations for individual GCPs, mean value, and total error compared to the Helmert transformation. This can also be observed in the visual comparison of the georeferencing result of Winsen castle in Fig. 11.

Due to the significantly different results obtained from the two types of transformations, it is evident that the scanned map exhibits substantial distortions that can be corrected through the use of a 3rd degree polynomial transformation. Additionally, there is a possibility that there may have been major errors in the measurement of GCPs, which went undetected. To investigate this further, a total of 12 distances were measured in both, the non-georeferenced orthophotos and the scanned map for comparison purposes. These distances are presented in Fig. 12 and detailed in Table 5, which includes the measurements as well as their deviations from the reference values.

(a) Helmert transformation　　　　　　　　　　　　(b) 3rd degree polynomial transformation

Fig. 11 Visual comparison of the georeferencing result between Helmert transformation (**a**) and 3rd degree polynomial transformation (**b**) on the data set of the Nikon D7500 with a 50 mm lens showing a large offset in the map (left)
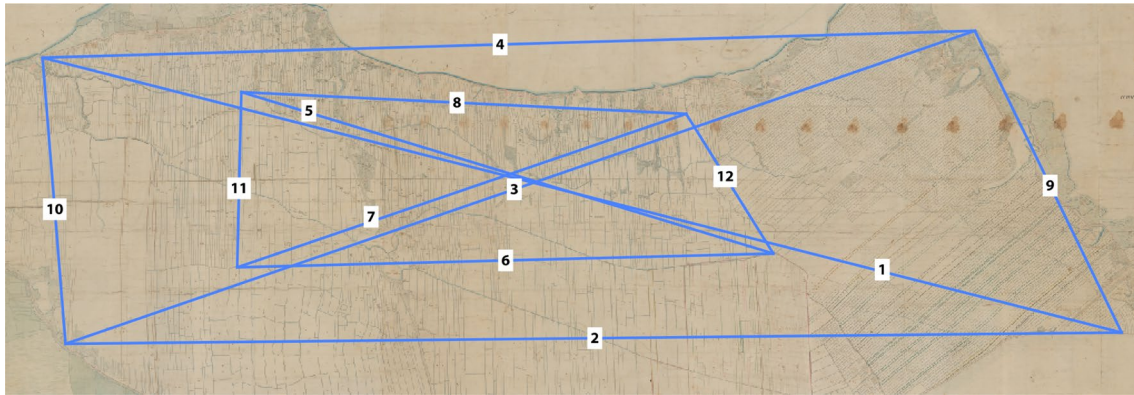
Fig. 12 Overview of measured distances in the scanned map and in the orthophoto of the Nikon D7500 with 50 mm lens (see also Table 5)

Table 5 Differences between distances (see Fig. 12) measured in the scanned map and in the orthophoto of the Nikon D7500 with 50 mm lens

No	Distance in map scale [m]			Distance in nature [m]		
	Scanned map	Ortho D7500	Deviation	Scanned map	Ortho D7500	Deviation
1	4.486	4.402	0.084	8771.373	8607.598	163.775
2	4.252	4.145	0.107	8314.651	8105.065	209.587
3	3.875	3.826	0.049	7577.737	7481.297	96.439
4	3.755	3.719	0.036	7343.070	7272.071	70.999
5	2.240	2.244	− 0.004	4379.725	4387.881	− 8.156
6	2.159	2.151	0.008	4222.336	4206.030	16.306
7	1.912	1.912	0.000	3738.660	3738.693	− 0.033
8	1.793	1.802	− 0.009	3505.737	3523.601	− 17.864
9	1.360	1.344	0.016	2659.800	2628.035	31.764
10	1.166	1.177	− 0.011	2279.189	2301.486	− 22.298
11	0.712	0.719	− 0.007	1391.687	1405.921	− 14.234
12	0.667	0.665	0.002	1304.456	1300.330	4.126

In each case related to the dimensions of the historical map (not georeferenced) and to the dimensions in nature (georeferenced)

The differences observed in the four longest distances are quite significant, but they include a wide range of variations, particularly for distances 5–12 (as shown in Table 5). However, no discernible systematic distortion effect can be identified based on the length of the distances. The differences summarised in Table 5 confirm the presence of the distortions in the scanned map when using the Helmert transformation for georeferencing. Given the high deviations associated with the Helmert transformation, this method can be deemed unsuitable for georeferencing the scanned map. On the other hand, georeferencing using the 3rd-degree polynomial transformation yields results that are comparable to those obtained from photogrammetric data sets. Therefore, this method can be considered suitable for georeferencing purposes. The georeferenced version of the scanned map, along with the Nikon D7500 equipped with a 50 mm lens, exhibits a similar ground resolution due to downsampling. However, the georeferenced scanned map shows more details and fewer imperfections such as bumps, cracks, and creases. Additionally, there is a more uniform illumination across the image, as depicted in Fig. 13. If the scanned map had been georeferenced at its full resolution, it would have been possible to achieve a higher ground resolution of 0.16 m/px instead of 0.67 m/px.

To compare the historical scales depicted on the digitised map with values provided in literature, a sample of four out of the six scales present on the map was analysed. The distances measured on these scale bars of the map correspond to 100 Calenberg rods, with each rod equivalent to 4674 m as mentioned in Sect. 2. However, the other two scales were not examined as they pertain to a profile drawing of the dyke that was created at a different scale. Unfortunately, information regarding the scale numbers is not available on the map.

The distances were measured in georeferenced orthophotos of the Nikon D7500 with 50 mm lens using the results of both the Helmert and 3rd degree polynomial transformation

Fig. 13 Comparison of a section of the scanned map and the orthophoto of the Nikon D7500 with 50 mm lens

Table 6 Measured distances in the scale charts in comparison with the target distances including calculated map scale

Nominal distance		Measured distance			Deviation		Scale number		
No.	[100 rods in m]	Helmert	Polynom 3	Non-georef	Helmert	Polynom 3	Helmert	Polynom 3	Non-georef
1	467.4	499.836	498.329	0.2558	− 32.436	− 30.929	1954	1949	1828
2	467.4	469.120	462.479	0.2401	− 1.720	4.921	1954	1926	1947
3	467.4	470.703	468.408	0.2411	− 3.303	− 1.007	1952	1943	1939
4	467.4	467.237	462.125	02392	0.163	5.276	1953	1932	1954
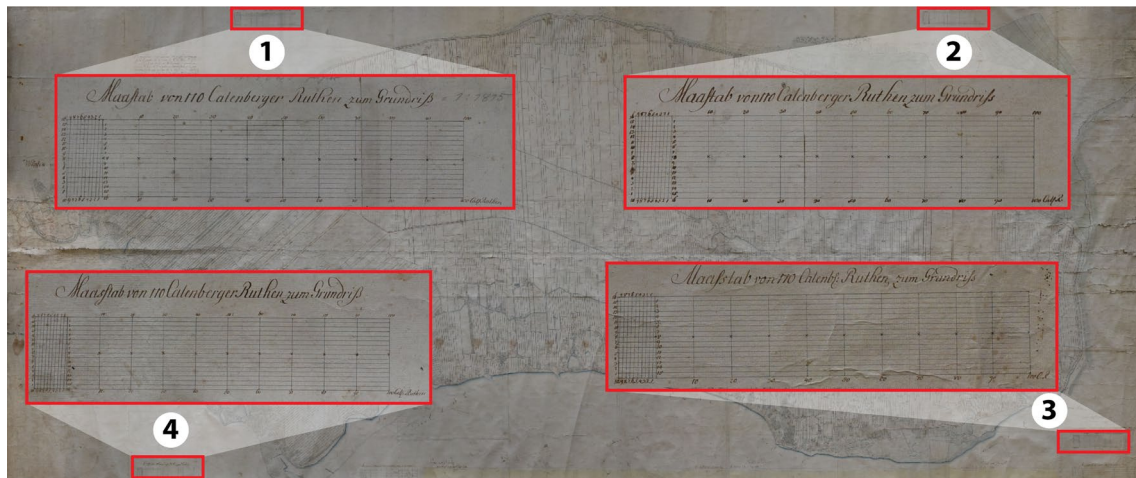
Fig. 14 Overview of the distances measured in the scale charts in Table 6 (enlarged sections are not shown in uniform scale)

methods. Additionally, distances were measured in the non-georeferenced orthophoto of the same data set to determine the map scale using these values later on. For each case, 100 Calenberg rods were measured at the upper and lower edges of the scale bars, and then averaged arithmetically. The measured distances are listed in Table 6, while the numbering of the scale bars is illustrated in Fig. 14.

The differences between the calculated nominal and measured distances are relatively small for scales 2, 3, and 4, ranging from a few decimetres to meters for both transformation methods. However, significant differences were observed at scale 1, with deviations of over 30 m for both transformation methods. These measurements were verified through multiple checks, confirming that the scale bar on the historical map was indeed drawn incorrectly. To further validate this finding, the four scales were overlaid in Adobe Photoshop using the copy-into mode. Scales 2, 3 and 4 are almost identical in height and width. In contrast, scale 1 had a similar height but differed significantly in width compared to the other scales. This observation further

supports the assumption that scale 1 was inaccurately drawn on the map.

The scale numbers in Table 6 were determined by dividing the measured distances in the respective transformation method by the measured distances in the non-georeferenced orthophoto for both Helmert and polynomial transformation. In the column "non georef." of Table 6 the nominal distance for 100 rods was compared to the measured distances in the non-georeferenced orthophoto. It can be observed from Table 6 that the calculated scale numbers for the Helmert transformation are all very similar, as the generated orthophoto was not distorted by this georeferencing process. However, this was not the case for georeferencing using the polynomial transformation. The calculated scales for the non-georeferenced orthophoto also indicate that scale 1 has a significant deviation compared to the other scales, whereas the scale numbers for the drawn scales 2, 3, and 4 show only minor deviations from each other. Considering all these findings in Table 6, it can be inferred that the historical map was likely drawn at a scale of approximately 1:1950.

7 Conclusions and Outlook

This contribution describes the successful digitisation and georeferencing of an oversized historical map of the Bailiwick of Neuland near Winsen an der Luhe in Germany using photogrammetric methods. The workflow, starting from image data acquisition to data processing and georeferencing, is presented along with investigations into geometric accuracy. To digitize the map, structure-from-motion (SfM) photogrammetry was employed using different camera systems. Agisoft Metashape software was used to generate digital orthophotos, which allowed for the mathematical compensation of unevenness on the map caused by bumps, coves, small cracks, and creases through orthogonal rectification. The georeferencing of the digital orthophoto was conducted using ground control points measured in official current digital orthophotos from the national survey of the state Lower Saxony, with a ground sampling distance of 20 cm. Two transformation methods, Helmert and 3rd-degree polynomial transformations, were employed for the computation of georeferencing. Despite the challenges posed by changes in the landscape over the centuries, the small deviations at the GCPs (ranging from 2.5 to 5.0 m) depending on the transformation method used indicate the high geometric quality of the historical map and the appropriate photogrammetric method. It is worth noting that significant differences in georeferencing accuracy were not observed among the investigated data sets. The best results in terms of quality and accuracy were obtained with the georeferenced orthophoto captured using a Nikon D7500 with 50 mm lens. This can be attributed to an optimal photo scale and the highest resolution achieved with this particular setup.

In contrast to the orthophotos generated through SfM photogrammetry, a professionally scanned map was used for accurate investigations of the georeferencing. When using the Helmert transformation for georeferencing the scanned map, large errors were observed at individual ground control points, ranging from several dozen meters up to 178 m. This indicates significant distortion in the composite of the scanned map. However, after georeferencing using the 3rd degree polynomial transformation, the results of the scanned map became comparable to the photogrammetric data sets. This can be attributed to the transformation method, which rectifies distortions based on GCPs. Despite the initial distortions in the scanned map, they were effectively corrected through this transformation method.

In addition to the georeferencing accuracy, the drawn scales on the map were also analysed by comparing measured distances with the nominal distance of 100 Calenberg rods. For three out of the four scales, deviations in the meter range were found, which can be considered negligible. However, it was observed that one scale had been grossly misdrawn, as it includes high deviations. Based on these findings, it was determined that the map was originally drawn at a scale of approximately 1:1950. This information provides valuable insights into the accuracy and reliability of the map's measurements and can be used to assess its suitability for various applications.

In future work, the historical map can be effectively used for automated vectorization of its content. Areas with predominantly linear objects such as parcel boundaries or ditches are particularly well-suited for this task. Automated methods can accurately extract these features from the map. However, more challenging areas may include settlement objects, which may require manual post-processing. This is also true for areas where visible distortions such as kinks, cracks, or dirt are present. These areas may be less suitable for automated vectorization and may require human intervention to ensure accurate representation. The topic of vectorization of historical maps is currently an important area of research. Schlegel (2023) describes an efficient and comprehensive workflow for semi-automated information extraction from large-scale historical maps. Yizi et al. (2021) present automatic vectorisation methods for historical maps using deep edge filtering and closed shape extraction. Iosifescu et al. (2016) introduce a comprehensive methodology for the automatic vectorization of raster historical maps. These studies provide valuable insights into the development of automated methods for extracting information from historical maps, which can greatly enhance their usability and accessibility in various applications.

References

AdV (Working Group of the Surveying Administrations of the Länder of the Federal Republic of Germany) (2020). Produkt- und Qualitätsstandard für Digitale Orthophotos. Version 4.1, https://www.adv-online.de/AdV-Produkte/Geotopographie/Luftbildprodukte/binarywriterservlet?imgUid=75419114-249e-4711-1fea-f5203b36c4c2&uBasVariant=11111111-1111-1111-1111-111111111111, last access 01. November 2023.

Affek A (2013) Georeferencing of historical maps using GIS, as exemplified by the Austrian Military Surveys of Galicia. Geogr Pol 86(4):375–390. https://doi.org/10.7163/GPol.2013.30

Agisoft LLC (2023). Agisoft Metashape User Manual—Professional Edition, Version 2.0. https://www.agisoft.com/pdf/metashape-pro_2_0_en.pdf, last access 01. November 2023.

Baiocchi V, Lelo K, Milone MV, Mormile M (2013) Accuracy of different georeferencing strategies on historical maps of Rome. Geographia Technica. 1(1):16

Ballarin M, Balletti C, Gottardi C (2015) Automatic systems for digitizing historical maps. e-Perimetron. 10(1): 21–29. https://air.iuav.it/retrieve/de164c2a-5b2e-60ee-e053-3a05fe0a7787/Ballarin_Balletti_Gottardi.pdf. Accessed 01 Nov 2023

Baltsavias EP, Patias P (1995) On the use of DTP scanners for cartographic applications. In 17th International Cartographic Conference.

Baltsavias EP, Waegli B (1996) Quality analysis and calibration of DTP scanners. International Archives of Photogrammetry and Remote Sensing (IAPRS). 31(B1): 13–19. https://www.isprs.org/proceedings/XXXI/congress/part1/13_XXXI-part1.pdf. Accessed 01 Nov 2023

Baltsavias EP, Haering S, Kersten T, Dam A (1998) Geometric and radiometric evaluation of the DSW300 roll film scanner. ISPRS J Photogramm Remote Sens 53(4):217–234

Brandolini F, Patrucco G (2019) Structure-from-motion (SFM) photogrammetry as a non-invasive methodology to digitalize historical documents: a highly flexible and low-cost approach? Heritage 2(3):2124–2136. https://doi.org/10.3390/heritage2030128

Chen Y (2023) Modern vectorization and alignment of historical maps: an application to Paris Atlas (1789–1950). Doctoral dissertation, IGN (Institut National de l'Information Géographique et Forestière), Paris.

Daniil M, Tsioukas V, Papadopoulos K, Livieratos E (2003) Scanning options and choices in digitizing historic maps. New perspectives to save cultural heritage. XIX CIPA International Symposium, WG 4 Digital Image Processing, Antalya, Turkey, 30 September–4 October 2003. https://www.cipaheritagedocumentation.org/wp-content/uploads/2018/11/Daniil-e.a.-Scanning-options-and-choices-in-digitizing-historic-maps.pdf. Accessed 01 Nov 2023

Flenniken JM, Stuglik S, Iannone BV (2020) Quantum GIS (QGIS): an introduction to a free alternative to more costly GIS platforms: FOR359/FR428, 2/2020. EDIS. https://doi.org/10.32473/edis-fr428-2020

ESRI Inc (2021) Fundamentals of georeferencing a raster dataset. https://desktop.arcgis.com/en/arcmap/latest/manage-data/raster-and-images/fundamentals-for-georeferencing-a-raster-dataset.htm, last access 01. November 2023.

Iosifescu I, Tsorlini A, Hurni L (2016) Towards a comprehensive methodology for automatic vectorization of raster historical maps. e-Perimetron 11(2):57–76

Kersten T, Lindstaedt M (2012) Automatic 3D object reconstruction from multiple images for architectural, cultural heritage and archaeological applications using open-source software and web services. Photogramm Fernerkund Geoinfo. 6:727–740. https://doi.org/10.1127/1432-8364/2012/0152

Kingsland K (2020) Comparative analysis of digital photogrammetry software for cultural heritage. Digit Appl Archaeol Cult Herit 18:e00157. https://doi.org/10.1016/j.daach.2020.e00157

Kost W (1955) Zur topographischen Kartographie im niedersächsischen Raum von 1764–1863. In: NV und Katasterverwaltung (Hrsg.) CF Gauß und die Landesvermessung in Niedersachsen. p 115–140.

Landesamt für Geoinformation und Landesvermessung Niedersachsen (2023) Einführung von ETRS89 und der UTM-Abbildung. https://www.lgln.niedersachsen.de/startseite/geodaten_karten/afis_alkis_atkis/etrs89_utm/einfuehrung-von-etrs89-und-der-utm-abbildung-51708.html, last access 01. November 2023.

Niedersächsisches Landesarchiv (2022) NLA HA Kartensammlung Nr. 35 n/19 k—Profile zum Plan der Vogtei Neuland. https://www.arcinsys.niedersachsen.de/arcinsys/detailAction.action?detailid=v4542721&icomefrom=search, last access 01. November 2023.

Luft J, Schiewe J (2021) Automatic content-based georeferencing of historical topographic maps. Trans GIS 25(6):2888–2906. https://doi.org/10.1111/tgis.12794

Luhmann T (2018) Nahbereichsphotogrammetrie—Grundlagen, Methoden, Beispiele. 4., neu bearbeitete und erweiterte Auflage, Wichmann. p 783.

Luhmann T, Robson S, Kyle S, Boehm J (2020) Close range photogrammetry and 3D Imaging, 3rd edn. De Gruyter, Berlin. https://doi.org/10.1515/9783110607253

Podobnikar T (2009) Georeferencing and quality assessment of Josephine survey maps for the mountainous region in the Triglav National Park. Acta Geodaetica Et Geophysica Hungarica 44(1):49–66. https://doi.org/10.1556/AGeod.44.2009.1.6

Schlegel I (2023) A holistic workflow for semi-automated object extraction from large-scale historical maps. KN J Cartogr Geogr Inf 73:3–18. https://doi.org/10.1007/s42489-023-00131-z

von Schlieben WEA (1857). Vollständiges Hand- und Lehrbuch der gesammten Feldmesskunst (4. Auflage). Ernst'sche Buchhandlung.

Seebach W (1955) Aus frühen Zeiten der Vogtei Neuland. In: Schröter G (Hrsg), Harburger Kreiskalender. p 97–98.

Stößel L (2023) Digitalisierung und Georeferenzierung einer übergroßen historischen Karte der Vogtei Neuland (Winsen/Luhe) durch Photogrammetrie. Unpublished bachelor thesis, HafenCity University Hamburg. p 45.

Yizi C, Edwin C, Chazalon J, Mallet C, Dumenieu B, Perret J (2021) Vectorization of historical maps using deep edge filtering and closed shape extraction. 16th International Conference on Document Analysis and Recognition—ICDAR 2021, Proceedings. Springer International Publishing, Cham, pp 510–525. https://doi.org/10.1007/978-3-030-86337-1